An OGI Based Unattended Natural Gas Leak Detection System by Utilizing the Power of Machine Learning and Computer Vision

Hritu Raj[a] and Gargi Srivastava[b]
Rajiv Gandhi Institute of Petroleum Technology, in Jais, Amethi, Uttar Pradesh, India
{*hritur, gsrivastava*}*@rgipt.ac.in*

Keywords: Natural Gas, Optical Gas Imaging, Gas Leak, Convolutional Neural Network, Computer Vision, Climate Change.

Abstract: In a climate-constrained future, reducing natural gas emissions is essential to prevent undermining the environmental benefits of using natural gas over coal. Although optical gas imaging (OGI) is widely used for detecting natural gas leaks, it is often time-consuming and relies on human intervention for leak identification. This study presents an operator-less solution for automated leak detection using convolutional neural networks (CNNs). Our approach utilizes a dataset of natural gas leaks to train a CNN model for automated plume recognition. We begin by gathering 32 video clips labeled with gas leaks from the FLIR dataset, which covers a variety of leak sizes (50-1800 g/h) and video capture distances (4.2-18.3 m) .Two background removal techniques were applied to isolate the gas plumes. A modified CNN model, trained with a combination of natural gas and smoke images from Kaggle, was then used to detect the plumes in the video frames. Our trained model was evaluated against other algorithms based on optical flow, showing impressive performance. Our CNN model achieved an accuracy of 99% in detecting medium/large leaks and 94% for small leaks. This approach offers a promising method for high-accuracy natural gas leak identification in real-world OGI assessments.

1 INTRODUCTION

Natural gas is a significant energy source, contributing 36.1% to America's energy output in 2023 (EIA, 2024). Its extraction has increased due to modern, low-cost drilling methods (Shakya et al., 2022), and the growing demand for gas-operated energy and heating facilities (Khallaghi et al., 2020) further integrates it with electricity generation systems. The rise in natural gas usage and production is partly driven by increased demand for heating in homes and businesses (Li et al., 2021), contributing to a reduction in coal dependence for electricity generation, which has decreased from 14.63% in 2019 to 12.7% in 2023 (FAQs, 2024). However, the environmental impact of natural gas is controversial (Brehm, 2019). While it has a lower environmental impact than coal when burned, it has a higher global warming potential if released without combustion, being 36 times more harmful than coal (GWP, 2023). Gas leaks from the oil and gas sector have been under-reported (Alvarez et al., 2018), and irregular large sources may account for a significant portion of emissions (Vaughn et al., 2018). Notably, the top 5% of leaks are responsible for 50-60% of total emissions (Brandt et al., 2016).

Regular gas leak detection is required for power plants in the U.S. and Canada. Leak detection and localization (LDAR) often use EPA Method 21 or infrared optical gas imaging (OGI) (Method21, 2023). Despite OGI's effectiveness, challenges remain, including high labor costs, impracticality for continuous monitoring, and inconsistent results due to operator skill (Ravikumar et al., 2018), (Yuan et al., 2017).

To address these issues, this research uses convolutional neural network (CNN)-based algorithms to analyze infrared imagery for automatic methane leak detection. This approach eliminates the need for human intervention and could enable automated detection. Few automatic systems are available, and comprehensive studies of their limitations and potential applications are lacking.

Our process for automated leak detection includes five phases: constructing a dataset with annotated clips of gas leaks of varying sizes and conditions; training a CNN to detect leaks in video frames; testing background removal techniques; evaluating the

[a] https://orcid.org/0000-0002-4907-8314
[b] https://orcid.org/0000-0001-6770-561X

Raj, H. and Srivastava, G.
An OGI Based Unattended Natural Gas Leak Detection System by Utilizing the Power of Machine Learning and Computer Vision.
DOI: 10.5220/0013345600003905

In *Proceedings of the 14th International Conference on Pattern Recognition Applications and Methods (ICPRAM 2025)*, pages 823-830
ISBN: 978-989-758-730-6; ISSN: 2184-4313

accuracy of automated detection under different conditions; comparing the CNN model with traditional optical flow techniques; and computing detection accuracy from various distances for different leak sizes.

2 RELATED WORK

2.1 Optical Gas Imaging

As mentioned above, OGI technique encounters several challenges. (1) The effectiveness of OGI is significantly impacted by the imaging range (Ravikumar et al., 2017). Imaging at a distance greater than ten meters significantly decreases OGI's efficiency. (2) Environmental factors like wind direction, temperature, and speed differences also play a role. Only a few commercial devices can be used for automated leakage detection with camera footage. With the help of ExxonMobil Research Qatar and Providence Photonics, an attachment for the FLIR Gas camera was developed for unsupervised remote monitoring of natural gas plumes(Abdel-Moati et al., 2013). Another firm, Rebellion Photonics, provides real-time detection using a hyper-spectral vision sensor that can differentiate between various gaseous molecules. (4) Detection results from conventional infrared cameras are purely qualitative. Hyperspectral infrared cameras can measure leak flow by monitoring uninterrupted spectral information for every pixel's intensity. The difference between RGB and thermal images is shown in Figure 1.

2.2 Smoke Detection

Scientists in computer vision and image processing have produced numerous articles on smoke detection. Similarities between natural gas plumes and smoke can be seen in their ethereal quality, ability to spread, and erratic movement. While thermal sensors are used to image hydrocarbon plumes, visual spectrum sensors capture smoke in all its colors. Color models, change identification, pattern analyses, and machine learning approaches (Hsu et al., 2018) are popular methods for detecting smoke emissions. We will evaluate and compare these models. Color modeling is based on the saturation or distribution of intensity values in an image. Reduced color saturation helps detect smoke pixels. (2) Motion recognition techniques identify movements or changes. The entropy of optical flows has been examined, and dazzling pixels used to outline edges. (3) Texture detection utilizes wavelet transform and other parameters to extract feature vectors, which are then used for classification (Ye et al., 2015). (4) Machine vision approaches for smoke detection are also explored, including CNNs (Frizzi et al., 2016).

2.3 Machine Learning

The environmental and energy-related applications of deep learning are numerous, in the field of wind energy, solar energy, energy cost predictions, etc. However, research on deep learning for natural gas leak detection is limited.

This article uses deep learning techniques to analyze images of natural gas leaks captured by Gas cameras. For tasks like object identification, voice recognition, video classification, etc., deep learning automatically extracts features from the dataset, unlike standard machine learning algorithms that rely on human-created attributes. In deep learning, several layers are used, where the first few layers learn basic features like points, edges, and curves, while higher-level layers learn more complex characteristics. Convolutional Neural Networks (CNNs) are effective in image recognition and object classification, with models like Resnet, VGG-16, and Alexnet (Szegedy et al., 2015). Despite differences, these models share a common structure with an Input layer, multiple hidden layers, and an output layer. Pool-Convolution layers are typically used in the hidden layers, where convolution operations are followed by subsampling in the pooling layer, reducing data dimensions. The final output layer, often fully connected, computes the regression result or classification score for each class.

3 DATASET

To train a deep learning network, CNNs need a huge amount of data. To deploy CNN to the problem of identifying natural gas leakage, we have started assembling a big dataset, which contains annotated footage of natural gas leaks from a variety of leaking sources, including a broad range of plume sizes. Various environmental circumstances, camera angles, and imaging distances were used to film these videos, giving a comprehensive representation of the whole spectrum of possible leak situations. The categorization based on 6 leak sizes and 5 imaging distance are shown in Figure. 2 and Figure. 3.

Optical Gas Imaging camera is the basic requirement of this research, and the cost of these cameras are too high. Thus, we have taken the support of the FLIR website for building our dataset. We have gathered 32 clips of natural gas leak from FLIR-

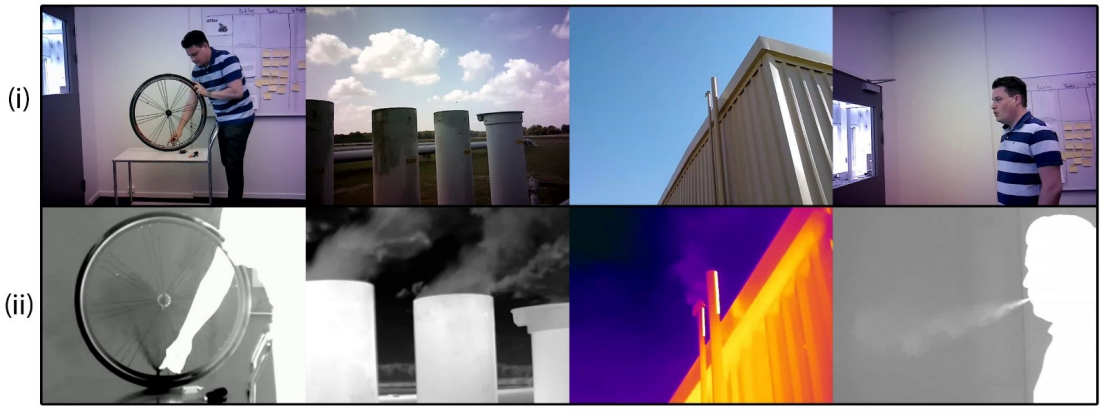

Figure 1: (i) Image taken from RGB camera and (ii) Image taken from FLIR gas imaging camera.

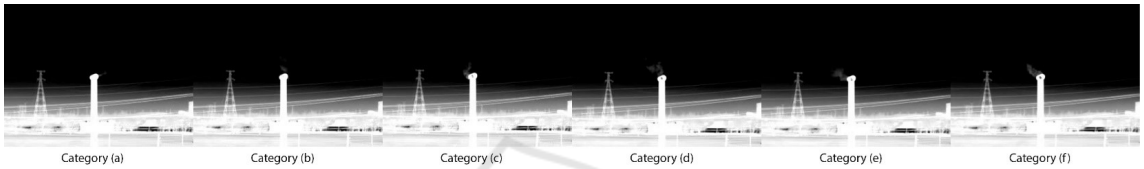

Figure 2: Leak size categorization (a to f).

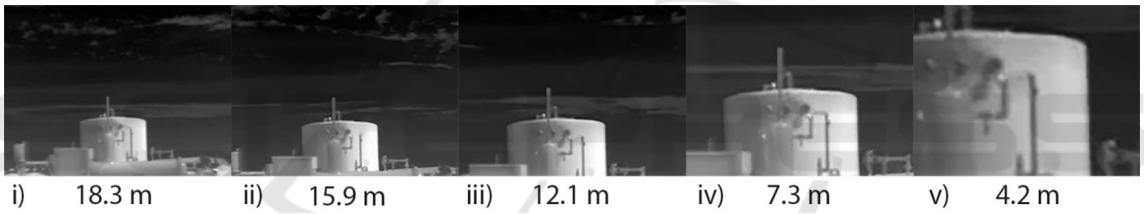

Figure 3: Footage taken at five imaging distances.

Conservator website. Then random 32000 frames are extracted for training the models. In this dataset we have also incorporated smoke dataset (Fire, 2024) to train for very large leak rates from longer distances. Hence, our dataset contains 837 images from smoke dataset and 32k frames gathered from FLIR conservator website (FLIR, 2024). The dataset is divided in 6 categories according to their leak sizes shown in Table 1.

Table 1: Categorization of dataset based on leak sizes.

Leak Type	Leak Rate gr/h	Leak Size
Category a	0-100	barely visible
Category b	101-500	very low
Category c	501-800	low
Category d	801-1200	moderate
Category e	1201-1600	high
Category f	1601 or greater	very high

Vegetation, steam, and vapor are all real-world phenomena that are not considered in our dataset. In addition, even at the lowest imaging distance, the greatest leak should not fill the whole field of view captured by the image sensor. In the future, research may be conducted considering these standards.

4 METHODOLOGY

An explanation of how our automated detection system works is provided below. Our CNN model is introduced, together with an image normalization technique and two new strategies for removing backgrounds. Our explanation of the CNN model is likewise quite detailed. And last, we propose a non-CNN baseline model that we may use to evaluate our outcomes.

4.1 Workflow

With 6 different binary classification situations, the automatic OGI-based technique gives a probability curve of proper assessment (a systematic technique to test the technology's effectiveness). A picture may be

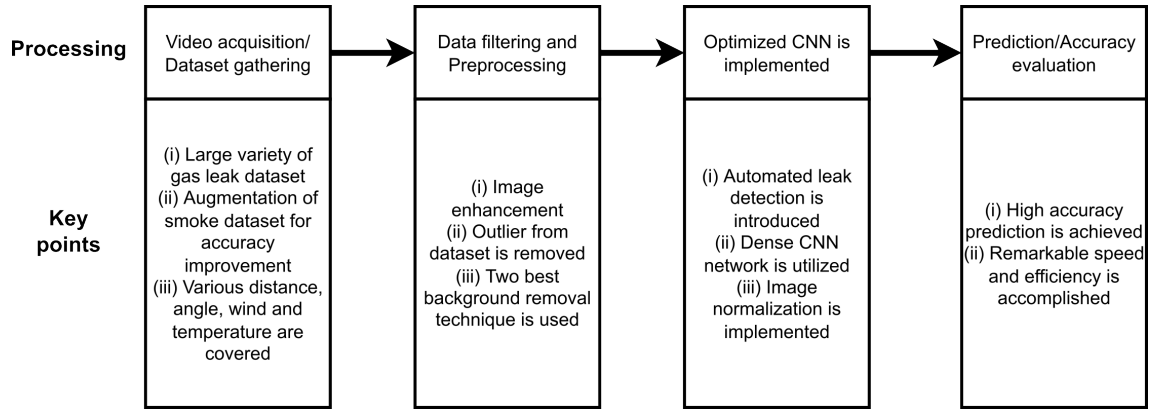

Figure 4: Processing steps and key points of the developed model.

placed into one of two categories using binary classification: either non-leak or leak image belonging to any of the 6 leak categories. This is done for all 5 imaging distances. Therefore, in our baseline scenario, we have 20 instances that each reflect the binary classification performance outcomes of 20 separate trained trials conducted at various distances from the camera and with varying leak sizes. Twenty individual training experiments are all carried out in the same manner. First, still images are taken out from videos and paired with their corresponding class names. Background removal and picture normalization are used to prepare the retrieved images for further processing. Each refined image is then fed into a trained convolutional neural network detection module. Finally, the percentage of properly detected frames by the algorithm is used to determine the accuracy of the predicted output. Data collection, image preparation (normalization and background removal), deployment of machine learning algorithms, and analysis of the probability distribution curve are all shown in Figure. 4. We will also go through how our research adds new insights to each procedure.

4.2 Background Subtraction

Background removal helps isolate the plume for detailed inspection. While perfect background removal would leave only the plume, real-world methods often retain some non-plume elements. We compare two background removal techniques—Mixture of Gaussians (MOG) and Gaussian Mixture Model (GMM)—against a baseline with no background removal. To perform background subtraction, we fuse frames from the no-leak category to create a static background for the leaked footage. For the fixed background scenario, all leak frames share the same background. A moving average of the last 150 frames is used to compute a static background for each frame. This method helps emphasize the gas cloud's variation by removing long-term background fluctuations. GMM background subtraction uses Gaussian distribution-generated pixel intensities (OpenCV, 2024), and an adaptive mixing algorithm determines the optimal number of Gaussian distributions for each pixel (Zivkovic and Heijden, 2006). Both background removal techniques yield nearly identical foreground images, as shown in Figure 5.

4.3 Image Normalization

A vital stage in deep learning, image normalization which ensures that all input images have a uniform pixel intensity distribution, allowing training algorithms to converge more quickly than they would with non-normalized data. The frames in our gas leak datasets are normalized by dividing each pixel by 255.

4.4 CNN Model

In this work, we use convolutional neural network (CNN) for making a clear distinction between leak imagery and other types of imagery using binary leak classification. Our CNN framework is built using standard procedures for creating CNN models. The data that are sent into the network are processed by a series of fully connected layers and a variety of ConvPool components. There is a convolutional layer, a batch normalization layer, a Rectified Linear Unit (ReLU) transfer function, a dropout regularization layer, and a max pooling layer in every ConvPool structure. Three-by-three-pixel filters are combined with the source frames in the convolutional layer. By using batch normalization after convolution, model training times are reduced while robustness is improved. Nonlinearity is brought into the network via the ReLU function (Nair and Hinton, 2010). With dropout, neurons are replaced or destroyed at ran-

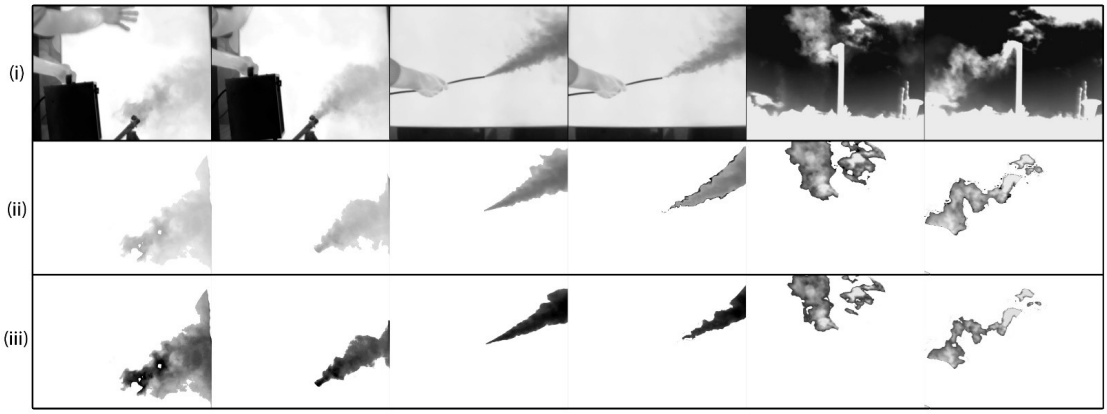

Figure 5: Background subtraction (i) Raw Image from FLIR camera, (ii) Subtraction using MOG and (iii) Subtraction using GMM.

dom during training as a kind of regularization (Hinton et al., 2012). It can help with stopping the CNN against overfitting. To decrease the size of the spatial frame presentation, the number of network parameters, and the amount of computation required, 2 by 2 max pooling is used (Ciregan et al., 2012). The first and second layer contain 8 and 16 filters respectively.

This processed input frame then goes through two further fully connected layers, one after the other, following the two Conv-Pool structures. There are 3600 neurons in the first layer, and 48 neurons in fully connected layer give outputs for 2 categories (leak and non-leak). Next, two probability scores, one for each of two classes, are generated using a SoftMax function, and the predicting label is calculated 0 (non-leak) and 1 (leak) shown in Figure. 6.

4.5 Model Setup

The learning rate for each factor is computed using the Adam optimizer (Ruder, 2016), an enhancement to stochastic gradient descent.

Experiment-specific training, validation, and testing datasets are shown in Table 2. The model is developed with the help of training data, hyperparameters are tuned using validation data, bias and variance are balanced with test data, and accuracy is reported using test data. 70% of the dataset from the second separator is used for training, while the remaining 30% is used for validation. The testing data are not included in the training data of the CNN classifier, and those are taken from different footage with different lighting conditions.

Table 3 shows how accuracy is calculated by calculating up the percentage of accurate binary leak and non-leak guesses (the total of the true negative and the true positive proportion over all data for testing). For each precision, we also determine its associated error.

Table 2: Data distribution for training, testing, and validation.

	Frames		
Distance (m)	Training	Testing	Validation
4.2	4000	1500	500
7.3	4000	1600	600
12.1	4000	1700	700
15.9	4000	1800	800
18.3	4000	1900	900

The size of the test dataset required a random 10-fold partitioning. Every fold in the test set is put through the testing procedure with the same best-trained classifier, yielding best accuracy scores.

Table 3: Method for accuracy calculation used in this research.

	PREDICTED	
ACTUAL	**No-Leakage**	**Leakage**
No-Leakage	True Negative	False Negative
Leakage	False Positive	True Positive

4.6 Baseline Model Method

We have created a non-deep learning approach so that we can compare its accuracy with our developed CNN model. Our detection accuracy benchmark for natural gas plumes is based on optical flow analysis. Between two frames, optical flow calculates how fast an item seems to be moving in the scene (OpenCV, 2024). Specifically, the dense optical flow method developed by Gunner Farneback is used to calculate optical flow at each pixel in the picture (Farnebäck, 2003). Areas with noticeable motion will be labelled as potential plume locations. Using the same configuration for training, testing and validation dataset as deep learning-based methods, the baseline approach

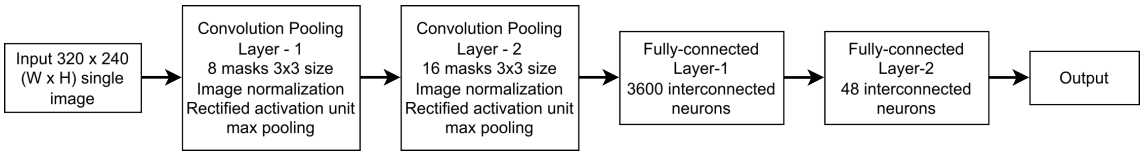

Figure 6: Proposed CNN architecture.

first applies the MOG background removal technique. The procedure for the baseline technique consists of four stages:

- Gunner Farneback's method is tuned using the training data such that the relocating areas visually correspond to the plume area.
- As a further step, we do a threshold analysis and arrive at two separate cutoffs. First, there is a line defined by the size of the movement (MMT). We classify a pixel as in motion if its estimated movement speed is greater than the MMT. It is presumed that any pixels in motion are plume pixels. Next is the plume area threshold (PAT). A leak plume is present in a picture if PAT is less than the count of moving particles, whereas the absence of a leak plume is indicated if the plume size is lower than the PAT. This is done by analyzing the training data's distributions of motion speeds and plume regions to establish a set of explorable thresholds.
- The validation set is used to iteratively examine the training data set footage for occurrences of MMT and PAT within each of the ranges observed. During testing, we look for the threshold that yields the best accuracy rate in the validation set and choose that one.
- The accuracy results of our leak category output on the dataset used for testing using the best threshold pair are reported.

5 RESULTS AND DISCUSSION

The findings of our implemented method are shown below for the 6 different classifications for leak or no-leak, each of which was carried out over five different imaging distances. The accuracy of predicted output is shown along the horizontal axis, beginning at 0.5, for each scenario. A randomly guessing method (tossing a coin) allocating frames to leak and non-leak states, given that we have tested each approach over a collection of leak or non-leak (50-50%) data.

First, we look at how removing the background effects the performance of our model, relative to a complex CNN architecture. We conduct a sensitivity study on the robustness of CNN model in the next set of data.

Results generated using two different background removal algorithms.

Firstly, we have checked the performance of background removal approach keeping the complexity of the CNN model constant.

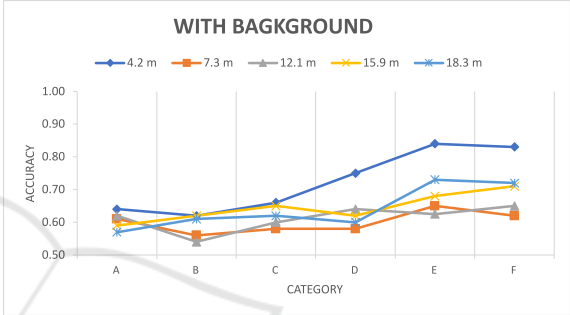

Figure 7: Detection accuracy of proposed model without background removal.

The diagram processed with the CNN algorithm and two distinct background reduction techniques. At the nearest capturing distance (4.2 m), larger leak sizes often lead to increased likelihood of correct evaluation when using the dataset keeping the background constant (Figure. 7). Maximum accuracy was 82% (percentages are rounded to the closest integer since the typical value for standard deviation is below 2%). As all values of the standard deviation are below 2.0%, which indicates that there is no variation in the trained CNN's performance over the training dataset with 10-folds. Videos captured 4.2 meters from the leak source have a plume that fills most of the frame, while non-leak footage include mostly the sky backdrop, making binary classification possible even without the need to remove the sky from the scene. However, when distance and leak size decrease, performance soon deteriorate to near random chance.

As can be seen in Figure. 8, the accuracy of Gaussian mixture model approach is greater than that of the fix background method. All 6 possible leak combinations have an accuracy of more than 82% at 4.2 m, while at 7.3 m, the accuracy of distinguishing between non-leak and leak class for C, D and E is greater than 96%. The accuracy may go up to 99% in these two scenarios. The gap between the curves for 12.1 m

and 15.9 m is much larger. Classification accuracy for determining leak vs non-leak situations is more than 90% at these distances for classes C, D and E. Except for the leak class 1 instance at the furthest distance, all 30 cases had standard deviations of less than 1.6% throughout the 10 test dataset folds.

Figure. 9 shows that when compared to static background, MOG-based background subtraction turns out better, although it still lags behind GMM mode. MOG and GMM approaches perform similarly in the two closest observations (capturing distance of 4.2 m and 7.3 m). At imaging distances greater than 10 meters, the accuracy disparity between the two approaches rises. The MOG-based background subtraction approach has an average accuracy 2.7%, 3.5%, and 6.2% poorer than the Gaussian mixture model subtraction method at distances of 12.1 meters, 15.9 meters, and 18.3 meters, respectively.

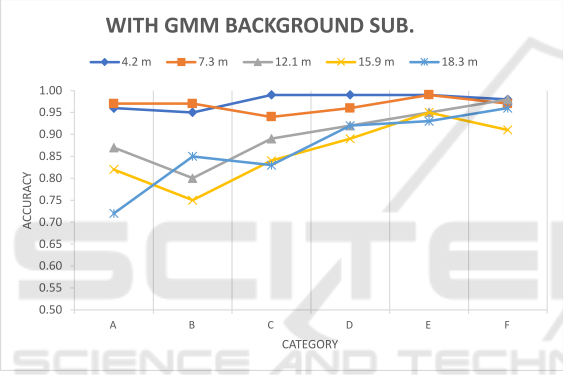

Figure 8: Detection accuracy of proposed model with background removal using GMM.

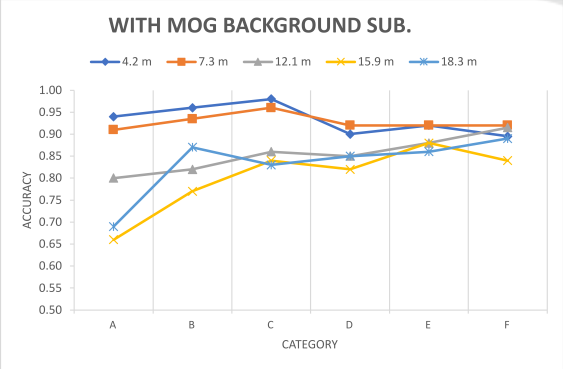

Figure 9: Detection accuracy of proposed model with background removal using MOG.

To the greatest extent, the success of automatic OGI-based techniques depends on the capturing distance. Our findings reveal that when imaging distance rises, there is a general downward change in the curve indicating assessment accuracy across 6 categories of leak and non-leak. When the capturing distance is larger, there seem to be fewer plume pixels available for utilization. Detection accuracy drops dramatically for the tiniest leakage over greatest distances.

It is important to note that the CNN model prediction results reported in this research for the automatic OGI-based detection techniques are not like the detection accuracy findings achieved for the OGI technology in past work that was run by humans. We cannot conclude that the algorithm is not as proficient as a person at spotting leaks. Two main factors contribute to this discrepancy is the human can use the highly sensitive settings of the OGI camera, which is much responsive to even poor movement of tiny leakage than the standard settings used in our research. The existence of hydrocarbon leak was defined by monitoring a leak footage, whereas in this study, we analyzed individual frames.

6 CONCLUSION AND FUTURE SCOPE

This study demonstrates the use of computer vision and deep learning techniques to automate natural gas leak detection with high accuracy. Using publicly available gas leak footage from the FLIR conservator website, we successfully tested our system. By integrating background removal with a CNN-based model, we identified leaks without needing a background image. The CNN model outperforms traditional leak detection methods. Our model achieves detection accuracy of up to 99%, especially over long distances with reduced complexity.

The accuracy of the algorithm depends on camera factors such as imaging range, temperature difference, and background motion. In future work, we plan to explore other model designs, including time-series models to track hydrocarbon leaks and plume movement. Given the numerous environmental variables affecting plume dispersion, combining physical models with machine learning could improve detection accuracy. These models could also help estimate the volume flux of gas plumes.

The use of ML-powered Optical Gas Imaging technology could reduce costs and speed up leak detection by installing it on survey trucks or surveillance cameras in leak-prone areas.

REFERENCES

Abdel-Moati, H. M., Morris, J. M., Ruan, Y., and Zeng, Y. (2013). Remote gas detection system using infrared

camera technology and sophisticated gas plume detection computer algorithm. *Proceedings - SPE Annual Technical Conference and Exhibition*, 6:4183–4193.

Alvarez, R. A., Zavala-Araiza, D., Lyon, D. R., Allen, D. T., Barkley, Z. R., Brandt, A. R., Davis, K. J., Herndon, S. C., Jacob, D. J., Karion, A., Kort, E. A., Lamb, B. K., Lauvaux, T., Maasakkers, J. D., Marchese, A. J., Omara, M., Pacala, S. W., Peischl, J., Robinson, A. L., Shepson, P. B., Sweeney, C., Townsend-Small, A., Wofsy, S. C., and Hamburg, S. P. (2018). Assessment of methane emissions from the u.s. oil and gas supply chain. *Science*, 361:186–188.

Brandt, A. R., Heath, G. A., and Cooley, D. (2016). Methane leaks from natural gas systems follow extreme distributions. *Environmental Science and Technology*, 50:12512–12520.

Brehm, P. (2019). Natural gas prices, electric generation investment, and greenhouse gas emissions. *Resource and Energy Economics*, 58:101106.

Ciregan, D., Meier, U., and Schmidhuber, J. (2012). Multi-column deep neural networks for image classification. *Proceedings of the IEEE Computer Society Conference on Computer Vision and Pattern Recognition*, pages 3642–3649.

EIA (2024). U.s. energy facts explained - consumption and production - u.s. energy information administration (eia).

FAQs (2024). Frequently asked questions (faqs) - u.s. energy information administration (eia).

Farnebäck, G. (2003). Two-frame motion estimation based on polynomial expansion. In Bigun, J. and Gustavsson, T., editors, *Image Analysis*, pages 363–370, Berlin, Heidelberg. Springer Berlin Heidelberg.

Fire (2024). Fire and smoke dataset — kaggle.

FLIR (2024). Flir conservator.

Frizzi, S., Kaabi, R., Bouchouicha, M., Ginoux, J. M., Moreau, E., and Fnaiech, F. (2016). Convolutional neural network for video fire and smoke detection. *IECON Proceedings (Industrial Electronics Conference)*, pages 877–882.

GWP (2023). Understanding global warming potentials — us epa.

Hinton, G. E., Srivastava, N., Krizhevsky, A., Sutskever, I., and Salakhutdinov, R. R. (2012). Improving neural networks by preventing co-adaptation of feature detectors.

Hsu, Y.-C., Dille, P., Sargent, R., and Nourbakhsh, I. (2018). Industrial smoke detection and visualization.

Khallaghi, N., Hanak, D. P., and Manovic, V. (2020). Techno-economic evaluation of near-zero co2 emission gas-fired power generation technologies: A review. *Journal of Natural Gas Science and Engineering*, 74:103095.

Li, N., Wang, J., Wu, L., and Bentley, Y. (2021). Predicting monthly natural gas production in china using a novel grey seasonal model with particle swarm optimization. *Energy*, 215:119118.

Method21 (2023). Method 21 - volatile organic compound leaks — us epa.

Nair, V. and Hinton, G. (2010). Rectified linear units improve restricted boltzmann machines vinod nair. volume 27, pages 807–814.

OpenCV (2024). Opencv: Background subtraction.

Ravikumar, A. P., Wang, J., and Brandt, A. R. (2017). Are optical gas imaging technologies effective for methane leak detection? *Environmental Science and Technology*, 51:718–724.

Ravikumar, A. P., Wang, J., McGuire, M., Bell, C. S., Zimmerle, D., and Brandt, A. R. (2018). "good versus good enough?" empirical tests of methane leak detection sensitivity of a commercial infrared camera. *Environmental Science and Technology*, 52:2368–2374.

Ruder, S. (2016). An overview of gradient descent optimization algorithms.

Shakya, S., Li, B., and Etienne, X. (2022). Shale revolution, oil and gas prices, and drilling activities in the united states. *Energy Economics*, 108:105877.

Szegedy, C., Liu, W., Jia, Y., Sermanet, P., Reed, S., Anguelov, D., Erhan, D., Vanhoucke, V., and Rabinovich, A. (2015). Going deeper with convolutions. *Proceedings of the IEEE Computer Society Conference on Computer Vision and Pattern Recognition*, 07-12-June-2015:1–9.

Vaughn, T. L., Bell, C. S., Pickering, C. K., Schwietzke, S., Heath, G. A., Pétron, G., Zimmerle, D. J., Schnell, R. C., and Nummedal, D. (2018). Temporal variability largely explains top-down/bottom-up difference in methane emission estimates from a natural gas production region. *Proceedings of the National Academy of Sciences of the United States of America*, 115:11712–11717.

Ye, W., Zhao, J., Wang, S., Wang, Y., Zhang, D., and Yuan, Z. (2015). Dynamic texture based smoke detection using surfacelet transform and hmt model. *Fire Safety Journal*, 73:91–101.

Yuan, M., Barron, A. R., Selin, N. E., al, Frank, S., Havlík, P., Tabeau, A., Ravikumar, A. P., and Brandt, A. R. (2017). Designing better methane mitigation policies: the challenge of distributed small sources in the natural gas sector. *Environmental Research Letters*, 12:044023.

Zivkovic, Z. and Heijden, F. V. D. (2006). Efficient adaptive density estimation per image pixel for the task of background subtraction. *Pattern Recognition Letters*, 27:773–780.